Applied Catalysis A: General 519 (2016) 68–77

Contents lists available at ScienceDirect

Applied Catalysis A: General

journal homepage: www.elsevier.com/locate/apcata

Innovative photo-Fenton catalysis by PE-FeOx films leading to methylene blue (MB) degradation: Kinetics, surface properties and mechanism

Laura Suárez [a], Huiyu Dong [a,b], Cesar Pulgarin [a,*], Rosendo Sanjines [c], Zhimin Qiang [b], John Kiwi [a,**]

[a] Ecole Polytechnique Fédérale de Lausanne, EPFL-SB-ISIC-GPAO, Station 6, CH-1015, Lausanne, Switzerland
[b] State Key Laboratory of Environmental Aquatic Chemistry, Research Center for Eco-environmental Sciences (RCEES), Chinese Academy of Sciences (CAS), 18 Shuangqing Road, Haidian District, 100085 Beijing, China
[c] Ecole Polytechnique Fédérale de Lausanne, EPFL-SB-IPMC-LNNME, Bat PH, Station 3, CH-1015, Lausanne, Switzerland

ARTICLE INFO

Article history:
Received 1 February 2016
Received in revised form 21 March 2016
Accepted 25 March 2016
Available online 26 March 2016

Keywords:
PE-FeOx synthesis
MB-discoloration
Visible light
XPS
AFM
XRD
Repetitive MB degradation
H_2O_2
Heterogeneous catalysis
ROS diffusion distances

ABSTRACT

This study reports an innovative preparation polyethylene-FeOx (PE-FeOx films) leading to the degradation of the methylene blue (MB) dye under low intensity sunlight/visible light (>400 nm). The intermediate highly oxidative radicals generated by PE-FeOx leading to MB discoloration/degradation in the presence of H_2O_2 were identified. The relative contribution to the MB discoloration by the Fe-ions leached from the PE-FeOx films into solution was determined quantitatively. This allows estimating the contribution of the heterogeneous and of the homogeneous leading to MB-degradation. The shift in the peak binding energy (BE) for Fe was detected by photoelectron spectroscopy (XPS) after the MB-degradation providing the evidence for *redox* catalysis occurring during MB-degradation at the PE-FeOx surface. The particle size and roughness of the PE-FeOx surfaces were determined by atomic force spectroscopy (AFM). The spectral properties of PE-FeOx films are reported and insight is provided for the mechanism of MB-degradation.

1. Introduction

The synthesis of environmentally friendly supported catalysts not needing high temperatures, organic solvents or expensive/sophisticated preparation methods is a research subject gaining in importance during the last decade [1]. During the last decade TiO_2 has been mostly used as the photocatalyst of reference to abate pollutants and bacteria in the presence of air (O_2), (H_2O_v) under band-gap irradiation <400 nm [2]. Recently some reviews have reported the discoloration/degradation of pollutants/dyes on polymers with adhesive catalytic layers [3–6]. This is due to the polymers low-cost, high availability, stability, flexibility and corrosion resistance. This study addresses the preparation, evaluation and surface characterization of a polyethylene Fe-oxide (PE-FeOx) polymer absorbing visible light up to ~520–530 nm [7]. Polymer thin films have shown to be flexible catalysts supports leading to catalysis/photocatalysis with acceptable kinetics and recently, some reviews have reported the degradation of organic compounds/dyes under UV/sunlight on polymers coated with TiO_2 and Au [8,9]. However a good adhesion of the photocatalyst semiconductor particles on the polymer surface starting with a colloidal suspension remains a problem since polymers do not present thermal resistance. Therefore, calcination of oxides/composites on polymers is not possible [10].

Methylene blue (MB) has been taken as the probe to test discoloration/degradation on PE-FeOx films avoiding the undesirable problem of the photocatalyst recovery encountered when using the Fenton reagent in solution. The PE is a low-cost, stable polymer presenting an inert surface and was selected as the substrate for the preparation of PE-FeOx absorbing light in the visible region. The band-gap of Fe_2O_3 has been reported as 2.2 eV with the posi-

* Corresponding author.
** Corresponding author.
E-mail addresses: cesar.pulgarin@epfl.ch (C. Pulgarin), john.kiwi@epfl.ch (J. Kiwi).

http://dx.doi.org/10.1016/j.apcata.2016.03.029
0926-860X/

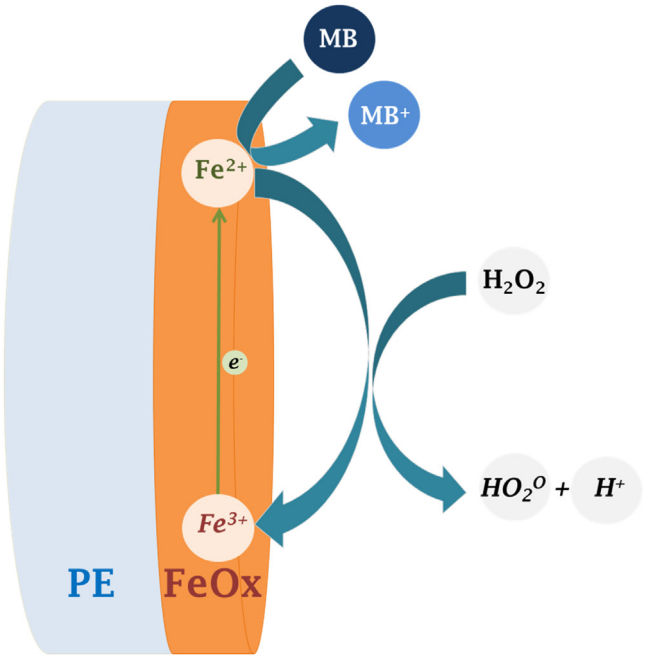

Scheme 1. Outline the MB-degradation mechanism on PE-FeOx films under sunlight/visible irradiation.

tions of the conduction band at 0.4 eV and of the valence band at 2.6 eV respectively [11]. The removal of MB by immobilized catalysts/photocatalysts presenting acceptable kinetics remains an important area of environmental research. MB is a stable dye that is not removed by conventional biological treatment and oxidation technologies and better performing catalyst absorbing light in the visible region should have to be developed to eliminate this dye [12–14].

Immobilized photo-Fenton processes on thin polymer films have been reported during the last decade. A Nafiion thin polymer film was reported to bind Fe^{3+}/Fe_2O_3 by electrostatic attraction avoiding the use of expensive Fe complexes/chelators when binding Fe-ions on polymer substrates [15]. Since Nafion is too expensive, a second study reported chelating Fe on negative maleic-anhydride fused on PE-films [16,17]. These studies show that immobilized Fenton catalysts led to the degradation of compounds beyond the narrow operational pH range around 3 required in Fenton processes in aqueous solution leading to the degradation of dyes. Later some colloidal preparations of Mn/Al/Fe oxides have been reported on PE-films leading to phenol degradation under light irradiation, but their reproducibility was not commented [18]. Supported rutile and iron oxides extruded and subsequently casted on PE films have been reported as photocatalysts [19]. The inactivation of bacteria on PE has been recently reported [20].

The novelty presented in this study addresses a) the innovative preparation of a stable PE-FeOx film presenting repetitive stable M-degradation performance, b) the identification of the intermediate radicals leading to MB-degradation by the use of appropriate scavengers, c) the estimation of both the lifetime and the diffusion length of the OH°-radical away from the PE-FeOx, d) the determination of the Fe-ions released from the PE-FeOx film within the MB degradation time providing the evidence for the Fe^{3+}/Fe^{2+} *redox* reactions, e) the nature of the Fe-Cl species left on the surface of the PE-FeOx film during the photocatalyst preparation and finally f) the shift by X-ray photoelectron spectroscopy (XPS) for the Fe, O and C-peaks during the MB-degradation providing further evidence for the *redox* process within the photocatalysis time.

2. Experimental

2.1. PE-FeO_x film preparation, film material, irradiation source, UV–vis spectrophotometry and total organic carbon (TOC) determination

Low-density PE-films were washed with Milli-Q water followed by acetone and dried at room temperature to eliminate surface contaminants. The PE film was then attached on a cylindrical Teflon support and immersed in a $FeCl_3{\cdot}7H_2O$ solution stirring for one hour at 80 °C. The films were left to dry at room temperature then washed with distilled water and dried at 80 °C for 15 min.

The low-density polyethylene (LDPE) used in this study is a highly branched low crystalline film with formula $H(CH_2\text{-}CH_2)_nH$. The (LDPE) 0.1 mm thick was obtained from Goodfellow, UK (ET311201). The film presented mechanical stability, had a density of 0.92 g cm^{-3} and was thermally stable up to 96 °C.

The photochemical reactor (see Supplementary material S1) was made out of glass and presented cylindrical shape with a diameter of 8 cm and contained an MB volume of 60 ml. Photolysis experiments were performed in a solar simulated Hanau Suntest Lamp with a tunable light intensity attachment equipped with an IR filter to remove IR radiation >800 nm. The UV-radiation <305 nm was removed by the Pyrex wall of the reaction vessels. The PE-FeOx films were positioned at the bottom of the reactor (see Supplement material S1). The MB-solution in the reactor was stirred during the photolysis. The height of the solution in the reactor was ~2 cm and the MB-solutions were pre-equilibrated for 30 min in the dark before each run. The absorbance of the MB-solutions was followed in Shimadzu UV-1800 spectrophotometer and the total organic carbon (TOC) was determined in a Shimadzu TOC 500 equipped with an ASI auto-sampler.

2.2. Intermediate ROS scavenging and determination of the Fe-ions leached out during MB discoloration

NaN_3 Fluka was used as oxygen singlet scavenger ($^1O_2$). 1,4-Benzoquinone (BQ) and methanol were used respectively as $HO_2^{\bullet-}/O_2^{\bullet-}$ radical scavenger and $OH^{\bullet}$- radical scavengers [12]. Ethylenediamine tetra-acetic acid (*EDTA-2Na*) was used as TiO_2vb hole scavenger [13]. Ferrozine was used to evaluate the total iron concentration leaching out during MB-degradation at 562 nm, in a solution buffered at pH 9.5. To differentiate the Fe(II)-species from the Fe(III)-species, the latter species was reduced to iron(II) with hydroxylamine hydrochloride and the absorbance taken after 3 min again at 562 nm.

2.3. Characterization of the PE-FeOx film microstructure and surface properties

By X-ray fluorescence (XRF) the Fe- and Cl-content on the PE-FeOx film was determined in a PANalytical PW 2400 unit. The atomic force spectroscopy (*AFM*) image signals were acquired in contact mode using a PSIA Xe-100 AFM. Silicon nitride cantilevers were used with feedback set points around 1.0 nN. The AFM scanner and position sensors were calibrated using standard samples from Mikromash. The experimental error in the roughness was below 10%. The mean surface roughness (RMS) was calculated for scanned areas of $4 \times 4\ \mu M^2$ and $20 \times 20\ \mu M^2$.

X-ray diffraction (XRD) patterns of the PE-FeOx films were recorded on a Philips X'Pert PRO diffractometer equipped with an X'Celerator detector and a Ni-filtered Cu K radiation operating at 40 kV and 40 mA. The X-ray photoelectron spectroscopy (XPS) of the PE-FeOx films was carried out in an AXIS NOVA photoelectron spectrometer (Kratos Analytical, Manchester, UK) provided for with monochromatic AlK_a ($h\nu = 1486.6$ eV) anode. The carbon C1s

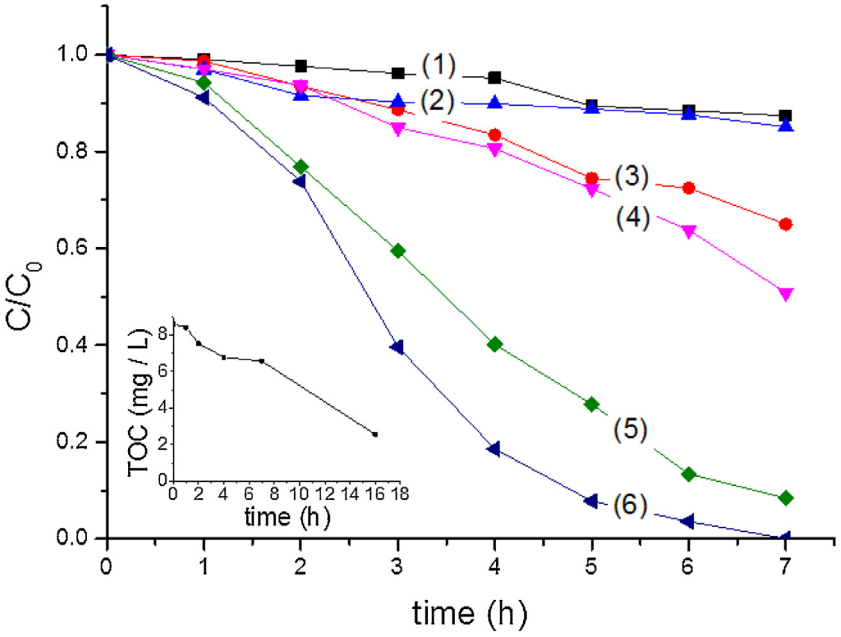

Fig. 1. Discoloration of MB (4×10^{-5} M) under different conditions at an initial pH 6 in solution: (1) MB alone under solar simulated irradiation (50 mW/cm^2), (2) PE-FeOx (Fe 0.30%) in the presence of H_2O_2 (10 mM) in the dark, (3) H_2O_2 (10 mM) under solar simulated irradiation (50 mW/cm^2), (4) Fe-ions in solution added to the MB-solution containing H_2O_2 (10 mM) under solar simulated irradiation (50 mW/cm^2), (5) MB discoloration on PE-FeOx (Fe 0.30%) in the presence of H_2O_2 (10 mM) under solar simulated irradiation (50 mW/cm^2) in the presence of a cut- off filter at 400 nm, (6) MB discoloration on PE-FeOx (Fe 0.30%) in the presence of H_2O_2 (10 mM) under solar simulated irradiation (50 mW/cm^2). Insert: TOC decrease of MB (4×10^{-5} M) in the presence of PE-FeOx (Fe 0.30%) film and H_2O_2 (10 mM). Suntest light intensity: 50 mW/cm^2.

line with position at 284.6 eV was used as a reference to correct for charging effects [21,22]. The surface atomic concentration was determined from peak areas using the known electrostatic correction factors according to Shirley [23].

3. Results and discussion

3.1. MB discoloration kinetics as a function of solution parameters, MB and H_2O_2 concentration and identification of the radical intermediates leading to MB-degradation

Fig. 1 presents the MB discoloration results under different experimental conditions. Fig. 1, trace 1 presents the discoloration of a solution MB (4×10^{-5} M) by itself under low intensity solar simulated radiation (50 mW/cm^2). Fig. 1, trace 2 shows the data for MB degradation by a PE-FeOx (Fe 0.30%) solution containing H_2O_2(10 mM) in the dark. In both cases practically no MB-discoloration was observed. A MB-discoloration of about 30% under solar simulated irradiation was attained within 7 h (Fig. 1, trace 3) for a solution made up by MB and H_2O_2. MB-discoloration within 7 h reaching 50% was observed upon addition of 1 mg/L Fe-ions/H_2O_2 (10 mM). In this case, the MB-degradation proceeds through a Fenton process in homogeneous solution as shown in Fig. 1, trace 4. Fig. 1, trace 5 shows a run under Suntest irradiation in the presence of a 400 nm cut-off filter. The visible light drives the MB-discoloration almost to completion within 7 h. Finally, Fig. 1, trace 6 presents the complete MB-discoloration by a PE-FeOx (Fe 0.30%) film in a solution containing H_2O_2 (10 mM). The insert in Fig. 1, shows the MB total organic carbon (TOC) of ~66% reduction for the solution reported in Fig. 1, trace 6. Different Fe-loadings on the PE-FeOx films did not significantly modify the MB-discoloration kinetics reported in Fig. 1, trace 6. The lowest Fe-loading of 0.17% (see Table 1) lead to a 70% MB-discoloration within 7 h compared to the complete discoloration induced by the PE-FeOx (Fe 0.30%) (see Supplementary material S2).

Table 1
Fe and Cl wt%/wt PE determined by X-ray fluorescence as a function of the $FeCl_3$ content during the preparation of PE-FeOx.

$FeCl_3 \cdot 7H_2O$ suspension concentration (g/L)	Fe wt%/wt PE	Cl wt%/wt PE
0	0.10	<0.20
0.5	0.17	<0.20
1	0.18	<0.20
10	0.30	0.31
20	0.37	0.39

Fig. 2a presents the MB-discoloration on PE-FeOx (Fe 0.30%) under simulated sunlight for MB-solutions presenting different concentrations. Similar end-points for the complete MB-discoloration proceeding through a mass transfer controlled reaction. Fig. 2b shows the MB discoloration kinetics being accelerated by increasing H_2O_2 concentrations. The effect of an increasing concentration of H_2O_2 can be understood by the Reaction (1) showing that higher concentrations of peroxide led to a higher concentration of OH•. The scavenging of the OH•-radicals on the MB-degradation is reported next in Fig. 3.

$$Fe^{2+} + H_2O_2 \rightarrow (Fe^{2+}...H_2O_2) \rightarrow Fe^{3+} + OH^- + OH^\bullet \quad (1)$$

Fig. 3 shows the scavenging of the radical intermediates generated in MB solutions under Suntest light irradiation. It is readily seen that a 0.2 mM methanol added to the solution quenches 55% of the MB-degradation and 0.2 mM NaN_3 quenches 60% of the observed MB-degradation. Fig. 3 shows that the OH•-radical and the O-singlet are the two moat active intermediates leading to MB-degradation. The $HO_2^{\bullet -}/O_2^-$ quencher *p*-benzoquinone and the EDTA-2Na hole quencher vb(h^+) did practically not preclude the MB-degradation under light irradiation. The absence of semiconductor effect by the PE-FeOx film on MB degradation becomes evident since the valence band holes vb(h^+) were not scavenged by EDTA-2Na. Another proof for the predominant effect for the photo-Fenton effect leading to the dye degradation comes from the observation that sunlight light doses between 30 mW/cm^2 and up

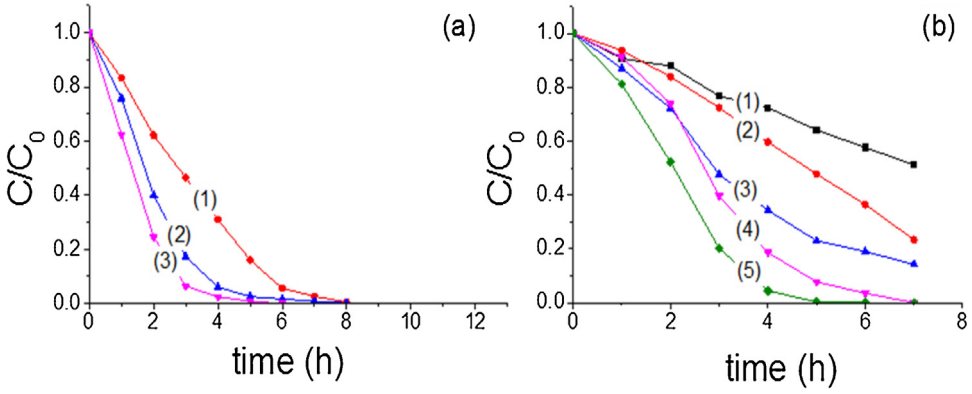

Fig. 2. (a) Discoloration of MB by on a PE-FeOx (Fe 0.30%) film irradiated under solar simulated irradiation (50 mW/cm^2) as a function of the initial MB concentration initial in a solution H_2O_2 (10 mM). MB: (1) 4×10^{-5} M, (2) 2×10^{-5} M, (3) 1×10^{-5} M. (b) Discoloration of MB by on a PE-FeOx (Fe 0.30%) film irradiated under solar simulated irradiation (50 mW/cm^2) as a function of the initial H_2O_2 concentration, MB 4×10^{-5} M, and the H_2O_2 concentration in traces: (1) 1 mM, (2) 2 mM, (3) 5 mM, (4) 10 mM, (5) 20 mM.

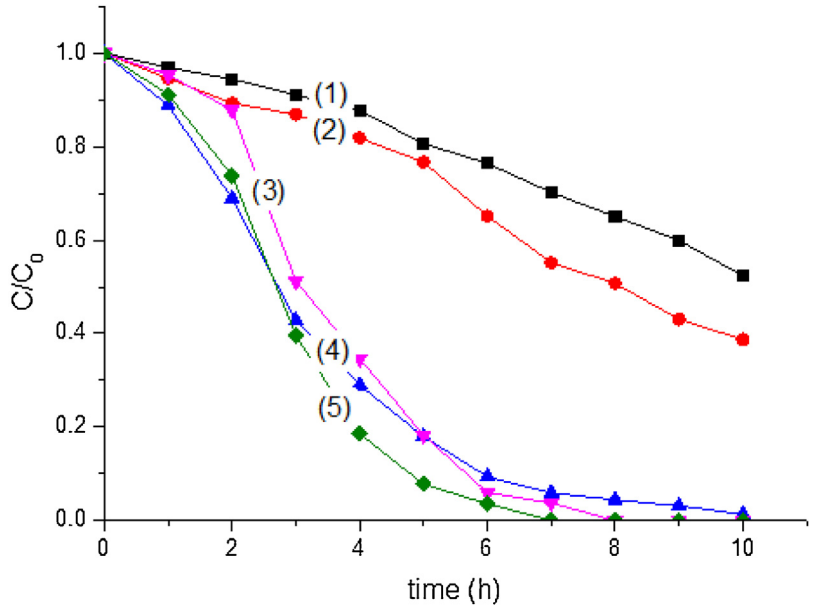

Fig. 3. Discoloration of MB (4×10^{-5} M) by means of PE-FeOx (Fe 0.30%) film, H_2O_2 (10 mM) and ROS scavengers under sunlight irradiation: (1) 0.2 mM methanol, (2) 0.2 mM NaN_3, (3) 0.2 mM *p*-benzoquinone, (4) 0.2 mM EDTA-2Na, (5) run without scavengers.

to 90 mW/cm^2 affected only marginally the rate of MB degradation (see Supplementary material S3).

With this information we suggest the nature of the radicals leading to MB-degradation [14–17].

$$Fe^{2+} + H_2O_2 \rightarrow Fe^{3+} + OH^{\bullet} + OH \quad k_1 = 76\ M^{-1}\ s^{-1} \tag{2}$$

$$Fe^{3+} + H_2O_2 \rightarrow Fe^{2+} + HO_2^{\bullet} + H^+ \quad k_2 = 2 \times 10^{-2}\ M^{-1}\ s^{-1} \tag{3}$$

$$Fe^{3+} + HO_2 \rightarrow Fe^{2+} + O_2 + H^+ \quad k_3 = 10^4\ M^{-1}\ s^{-1} \tag{4}$$

$$H_2O_2 + OH^{\bullet} \rightarrow HO_2 + H_2O \quad k_5 = 2.7 \times 10^7\ M^{-1}\ s^{-1} \tag{5}$$

$$Fe(OH)^{2+} + h\nu \rightarrow Fe^{2+} + OH^{\bullet} \tag{6}$$

$$Fe^{2+} + OH^{\bullet} \rightarrow Fe^{3+} + OH^- \quad k_4 = 4.3 \times 10^8\ M^{-1}\ s^{-1} \tag{7}$$

The degradation of MB due to the Suntest sunlight simulated alone is negligible as shown in Fig. 1, trace 1. The H_2O_2 decomposition leading to OH•-radicals under the experimental conditions used: $H_2O_2 + h\nu \rightarrow 2$ OH•-radicals are not important as shown in Fig. 1, trace 3 due to the low absorption coefficient of H_2O_2 > 305 nm close to 0.7 M^{-1} cm^{-1} [24]. Reactions (1)–(2) present the classical Fenton mechanism playing a role in MB-degradation. Reaction (3) seems not to be important since the amount of $HO_2^{\bullet}$ radicals produced is negligible during the MB-degradation as shown in Fig. 3, trace 3. During the MB-degradation the natural pH of the MB- solution of 6.0 was seen to decrease by 2–2.5 units as noted by the H^+-species in Eqs. (3)–(4) (see Supplementary material S4).

Fig. 2b shows that increasing the concentration of H_2O_2 (10 mM) to H_2O_2 (20 mM) led to a faster MB-degradation kinetics. Therefore, there was no scavenging of the OH•-radicals by the H_2O_2 as shown in Fig. 2b, trace 5. Eq. (6) shows the effect of light in the reduction of Fe^{3+} (or regeneration of Fe^{2+}) consistent with the data reported in Fig. 1, trace 2 [25]. No MB-degradation in the absence of light seems to take place due to the extremely slow rate of reaction for the conversion Fe^{3+}/Fe^{2+} noted in Eq. (2). Eq. (7) does not seem to proceed, since the pH within the degradation time moves to more acidic values and this excludes the formation of OH^-.

The MB-degradation kinetics was found to be faster at more acidic pH-values. An initial pH of 8.5 lead to a 50% MB-degradation within 7 h while a 100% degradation was attained at pH-values 6.8 and 5.0. At pH 4 the complete MB-degradation was completed within 5 h (see Supplementary material S5). At pH >4.5 the Fe(II/III)-aqua complexes on the PE-FeOx liberate OH•-radicals under light as

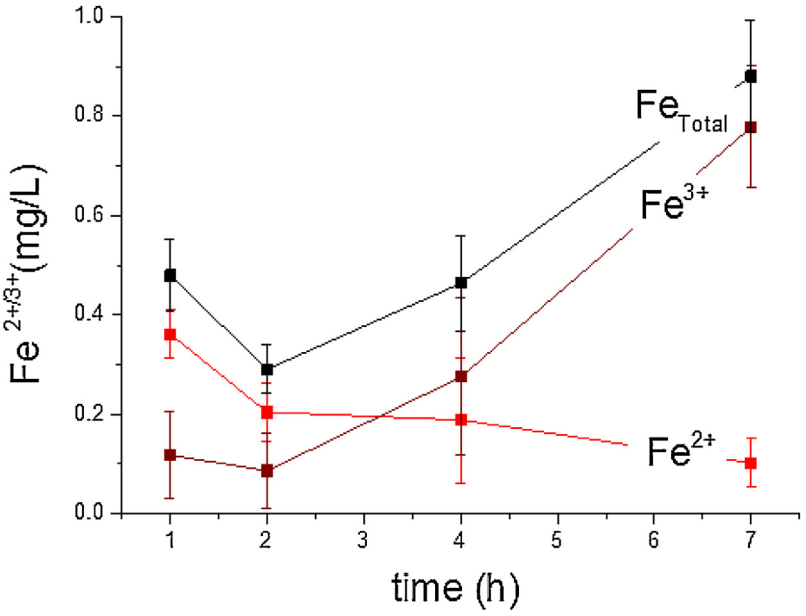

Fig. 4. Fe-ions released by the PE-FeOx (0.30%) film into the MB (4×10^{-5} M) solution containing H_2O_2 (10 mM), Suntest light intensity 50 mW/cm^2.

shown in Reaction (8) [26]. This reaction becomes faster as the pH becomes more acidic producing a higher amount of the Fe-hydroxy species $Fe(III/II)(H_2O)_6^{3+/2+}$.

$$Fe(III)OH(H_2O)_5^{2+} + H_2O + h\nu \rightarrow Fe(II)(H_2O)_6^{2+} + OH^{\bullet} \quad (8)$$

The FeOx film probably undergoes a *redox* reaction between MB and the Fe^{3+} on the PE-film leading to Fe^{2+} and the formation of the unstable MB^+-cation.

$$MB + [PE\text{-}Fe^{n}Ox] + h\nu \rightarrow [MB* \ldots Fe^{n}Ox]PE \rightarrow [MB^{+} \ldots Fe^{n-1}Ox]PE \quad (9)$$

The MB* excited singlet in Eq. (8) has been reported with a lifetime of 358 ps [27]. This excited singlet intercrosses subsequently to the triplet state with a lifetime of 4.6 ms. From this state an unstable MB^+-cation is formed responsible for the MB degradation/discoloration [28]. The *redox* reaction between MB and $Fe^{2+/3+}$ is shown to be accelerated by increasing amounts of H_2O_2 as shown above in Fig. 2b and is in agreement with earlier results reported by our laboratory [29]. Fig. 1 (insert) reports the total organic carbon decrease during MB-discoloration. This is an indirect indication of CO_2 generation (mineralization of MB). The MB generates short-lived organic acids branched or not preceding the final CO_2 mineralization step [30]. The last mineralization step of organic compounds proceeds due to the photo-Kolbe reaction. This reaction is outlined below in Eq. (10), where R is a short notation for the intermediate for the short carboxylic-acid in solution preceding the CO_2 evolution.

$$[RCOO\text{-}Fe^{3+}] \rightarrow [R^{\bullet}] + Fe^{2+} + CO_2 \uparrow \quad (10)$$

From the information presented in Figs. 1, 2 a,b and 3 in the text and in the Supplementary material S2–S5 (Section 3.1) a simplified MB-degradation mechanism under sunlight/visible irradiation is suggested in the Scheme 1 below:

The PE-FeOx film was prepared using $FeCl_3 \cdot 7H_2O$ as the iron and chloride source. The Cl^--anions on the film surface may as well play a role during the degradation of organic compounds as documented previously [31] leading to highly oxidative $Cl_2^{\bullet -}$ radicals:

$$Fe^{3+} + Cl^- \rightarrow FeCl^{2+} \quad (11)$$

$$Fe^{3+} + 2Cl^- \rightarrow FeCl_2^{+} \quad (12)$$

$$FeCl_2^{+} \rightarrow Fe^{2+} + Cl^- \quad (13)$$

$$Cl^- + Cl^{\bullet} \rightarrow Cl_2^{\bullet -} \text{and} ClOH^{\bullet} \quad (14)$$

3.2. Lifetime and diffusion distance of the OH•-radical away from the PE-FeOx intervening in MB-degradation

Fig. 3 shows that the OH•-radical is the most important oxidative radical leading to MB-degradation. Estimation of the OH°-radical lifetime takes into account: a) the rate of the reaction $Fe^{2+} + H_2O_2 \rightarrow Fe^{3+} + OH^- + OH^{\bullet}$, as noted in Eq. (2) $k_2 = 76\ M^{-1}s^{-1}$ and b) the reaction of OH° + MB (RH) → products ($k_2 \sim 10^{10}\ M^{-1}s^{-1}$). Inserting the solution parameters MB = 4×10^{-5} M, $H_2O_2 = 10^{-2}$ M, $Fe^{3+} = 2 \times 10^{-5}$ M (equivalent to 1 mgFe/L) leached in the solution during MB-degradation and knowing that in the quasi-stationary state the OH•-radical concentration is close to zero, allows to estimate a value of 0.38×10^{-10} M for the OH•-radical concentration (see Supplementary material S6). To estimate the OH•-radical mean-free path (x) away from the PE-FeOx surface, the Smoluchowski simplified approximation is used. Being D the diffusion of molecules with a low molecular weight like MB and $1/\tau$ the inverse of the encounter pair $\tau = 1/(k_{OH} + MB) \times [MB]$. Using the values in the relation $x^2 \sim D\tau$, the mean-free path is $x \sim 35$ nm (see Supplementary material S7).

3.3. Fe-leached out during MB-degradation and repetitive dye degradation

The Fe-ions leached into the solution during the degradation of the MB solution are shown in Fig. 4. The total Fe-ions leached out after 7 h was ~0.9 mg/L. This amount of Fe is close to the Fe-ions concentration added in the run reported in Fig. 1, trace 4, leading to a 50% MB-degradation within 7 h. Therefore, as the reaction time progresses, the PE-FeOx film would catalyze the MB-degradation through a progressively heterogeneous/homogeneous reaction. The Fe^{3+}-ions make up about 90% of the Fe-ions detected in the solution after 7 h, while the Fe^{2+}-ions make up the residual Fe-ions as shown in Fig. 4. This is expected due to two reasons: a) the solution contains H_2O_2 during the entire degradation process and b) the conversion in the dark of Fe^{2+} to Fe^{3+}-ions proceeds with

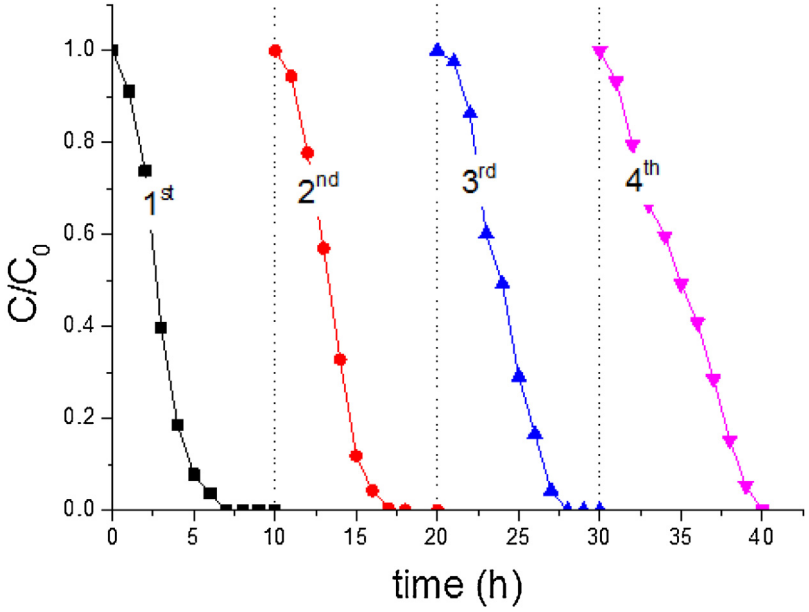

Fig. 5. Repetitive MB (4×10^{-5} M) discoloration on PE-FeOx (Fe 0.30%), H_2O_2 (10 mM), Suntest light intensity 50 mW/cm^2.

a rate $k_1 = 76\,M^{-1}s^{-1}$ while the back reaction to the Fe^{2+} proceeds with a slow rate of $k_2 = 2 \times 10^{-2}\,M^{-1}s^{-1}$ as noted by Eqs. (2) and (3) above in Section 3.1.

Fig. 5 shows repetitive MB-degradation cycles. The Fe^{3+}/Fe^{2+}-ions leached into the solution during the MB-degradation revert back to the PE-FeOx film surface containing the Fe-agglomerates after dye degradation. This is the way nature is cleaned either by a dark or photo-activated Fenton reagent in water bodies containing micro-molar peroxide/oxidative radical concentrations and Fe-ions [32,33].

3.4. Properties of PE-FeOx films: optical absorption, X-ray diffraction (XRD) particle size, film roughness and X-ray photoelectron spectroscopy (XPS)

Fig. 6 presents optical absorption of PE-FeOx films prepared with a different loading of Fe as shown in Table 1. As the Fe loading increases on the PE-film, the optical Fe d-d transition also increased. The onset of the Fe_2O_3 absorption at 550–600 nm (2.1–2.2 eV) is in good agreement with the values reported by Hardee and Bard [7]. The Fe_2O_3cb with a cb at 0.4–0.5 eV pH 0 *vs* SCE does not allow the reduction of O_2 (air) requiring potentials of ~0.16 eV [1,2] which would subsequently attack MB. This provides a further evidence for the MB-degradation occurring due to a photo-Fenton catalysis and not through to a light induced PE-FeOx semiconductor effect. The MB-degradation was due to the PE-FeOx film comprising a mixture of iron species. This will be shown by XRD next in Fig. 7.

By X-ray diffraction Fig. 7a shows the XRD run for the Fe-oxides peaks on the PE-FeOx films. Fig. 7b shows the XRD peak positions for the Fe and chloride species: FeOCl, $FeCl_2 \times 2H_2O$, $FeCl_2 \times 4H_2O$, $FeCl_3$ for: a) sample with a Fe 0.37%/0.39Cl% content and b) for a sample with a Fe 0.30%/0.31Cl% content. The possible involvement of Fe-ions and Cl^- species has been described in Eqs. (11)–(14) and the role of the highly oxidative radicals $Cl_2^{\bullet -}$ and $ClOH^{\bullet}$ may also be important during the MB-degradation due to the high reduction potential of the $Cl/Cl_2^{\bullet -}$ pair [31].

Fig. 8a shows AFM images of PE-FeOx (Fe 0.37%) film scanning an area ($20 \times 20\,\mu M^2$). The surface morphology shows micro-agglomerates of ~6 μm diameter size and present a roughness of RMS = 148 nm (see Table 2). The values for the RMS reported in Table 2 are the median in the Z plane of Z_{1a}–Z_{2a} shown in the right hand-side of Fig. 8a–d. The distance between the peaks and the valleys is taken for many particles in the agglomerates and the final values summation are averaged for resolutions of $4 \times 4\,\mu M^2$ or $20 \times 20\,\mu M^2$.

Fig. 8b shows that the agglomerates are formed by nano-particles with sizes 100–200 nm presenting a RMS = 78.4 nm in a scanning an area ($4 \times 4\,\mu M^2$) as noted in Table 2. The Fig. 8c shows AFM images for PE-FeOx (Fe 0.17%) film scanning an area ($20 \times 20\,\mu M^2$). The surface morphology shows the micro-agglomerates of ~10 μ with a roughness of RMS = 148 nm. This is a higher size dispersion compared to the values found for the PE-FeOx (Fe 0.37%) film. Fig. 8d show sizes ~100 nm for the nano-particles PE-FeOx films (Fe 0.17%). Scanning an $20 \times 20\,\mu M^2$ area renders an RMS = 60 nm (Table 2) while scanning an area $4 \times 4\,\mu M^2$ shows the presence of triangular shaped nano-particle of sizes ~100 nm and roughness RMS = 20.5 nm. Fig. 8a shows that decreasing in the Fe-content in the films leads to: a) lower surface roughness and b) an increase in the average particle size.

Fig. 9 presents the results of the XPS runs within the MB-degradation time. The Fe2p peak binding energies (BE) shift from 709.72 eV to 709.96 eV [21,22]. The shift towards higher BE for the Fe2p-states means that the Fe is being oxidized within the 10 h period. A new oxidation state appears since the BE displacement was >0.2 eV corrected for electrostatic charging effects [23]. Therefore, the MB-degradation involves concomitant *redox* Fe-reactions on the film surface. The O1s spectral shift in Fig. 9 from 530.18 eV to 530.48 eV involves a modest reduction to a O1s reduced species. This shows again *redox* processes during the MB-degradation time. The O1s are seen to be broad with multiple overlapping components. This makes it difficult to accurately quantify the oxygen chemical states [21,22]. O-species have been reported in metal oxides with different binding energies and their interpretation is not straightforward since the O1s binding energy of many metal-oxides falls within a narrow range. This is complicated by the presence organic C—O compounds and carbonates.

The *redox* reactions involving C1s-species during the MB-degradation are shown next in Fig. 9. A shift in the C-peak from 283.46 eV to 283.66 eV means an oxidation of the C1s-species -whatever their identity- on the topmost PE-layers during MB-degradation. This is to be expected in view of the nature of the

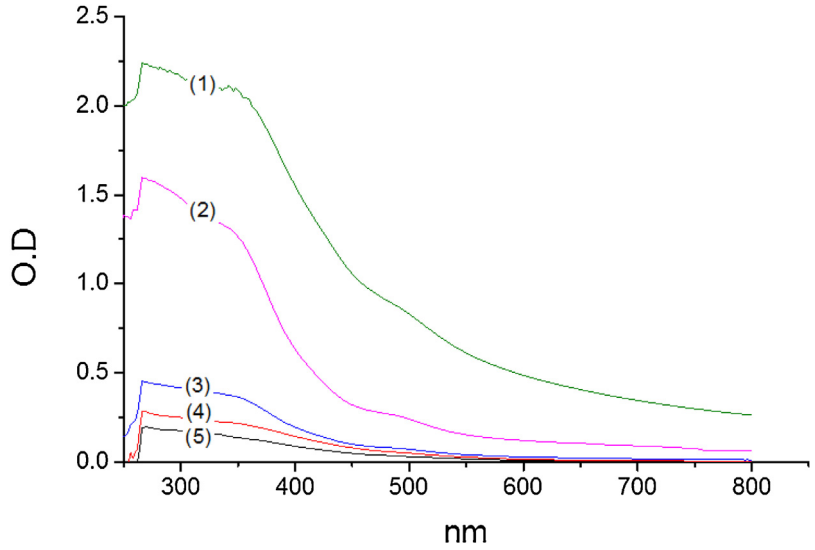

Fig. 6. Optical density (O.D) of PE-FeOx films: (1) 0.37 Fe wt%/wt PE, (2) 0.30 Fe wt%/wt PE, (3) 0.18 Fe wt%/wt PE, (4) 0.17 Fe wt%/wt PE, (5) 0.10 Fe wt%/wt PE.

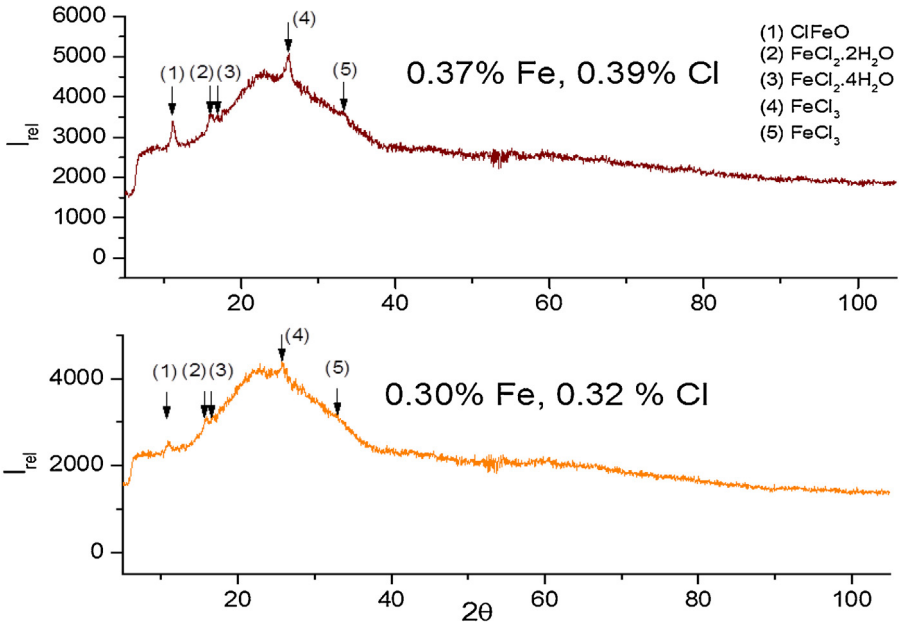

Fig. 7. XRD results PE-FeOx (Fe 0.37%) and for PE-FeOx (Fe 0.37%) matrix. The species containing FeClO are shown in the Figure caption.

Table 2
PE-roughness as a function of Fe loadings in the PE-FeOx film.

	Roughness Low resolution ($20 \times 20\ \mu M^2$)		Roughness High resolution ($4 \times 4\ \mu M^2$)	
	RMS (nm)	Average (nm)	RMS (nm)	Average (nm)
PE-FeOx, Fe 0.37%	148	120	78.4	63.3
PE-FeOx, Fe 0.17%	60.08	47.3	20.5	16.5

Fenton reagent Fe^{2+}/H_2O_2 that transforms instantaneously the Fe^{2+}-ions into Fe^{3+}-ions by contact with H_2O_2.

Table 3 shows the surface percentage atomic concentration of the elements making-up the PE-FeOx as determined by XPS. Previous to the XPS measurements, the PE-FeOx samples were contacted with MB in the dark for 30 min to deposit a fine layer of MB on the of PE-FeOx film. During 30 min the MB undergoes adsorption on the PE-FeOx film in the absence of H_2O_2 in the dark. At time zero, Table 3 shows the C-content is 82.03% and the C-content decreases afterwards due to the loss of C during the MB-degradation (see insert Fig. 1). The N-content found in the MB formulation is shown to decrease within the time of photocatalysis. The O-increases with time due to the generation of carboxylic acid intermediates in the solution. This is in agreement with results reported in reference [14]. Table 3 shows that the S-content decreases by more than 70% within the MB-degradation time. The Fe-content on the PE-FeOx surface is shown to increase since the topmost PE-FeOx surface is cleaned progressively from the dye during MB-degradation.

Fig. 5 shows stable repetitive cycling of the PE-FeOx film leading to MB-degradation and provides the proof that the surface of the PE-

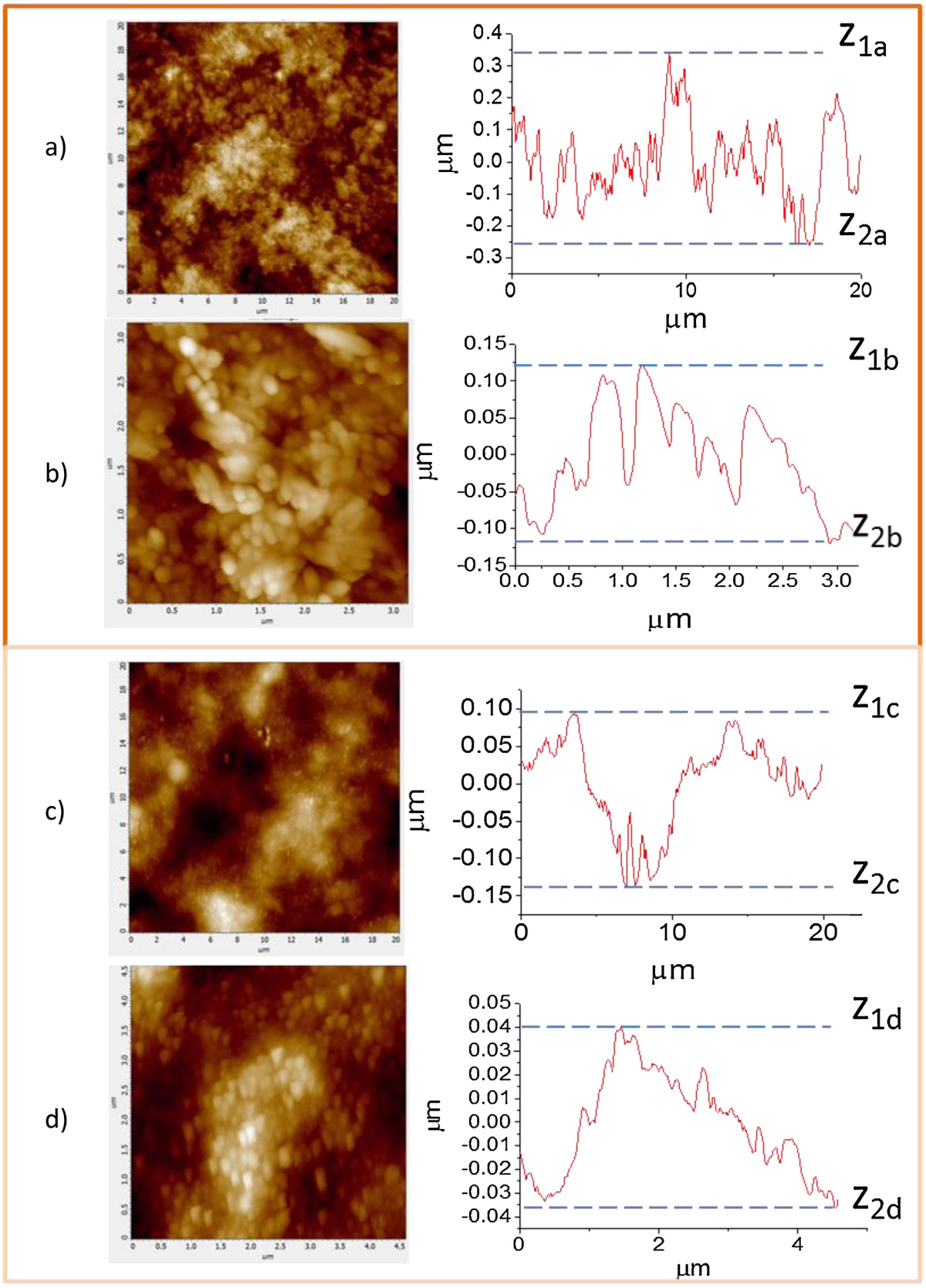

Fig. 8. (a) Roughness of PE-FeOx (Fe 0.37%) film taken at a roughness resolution ($20 \times 20\ \mu M^2$), (b) Roughness of PE-FeOx (Fe 0.37%) film taken at a roughness resolution ($4 \times 4\ \mu M^2$), (c) Roughness of PE-FeOx (Fe 0.17%) film taken at a roughness resolution ($20 \times 20\ \mu M^2$), (d) Roughness of PE-FeOx (Fe 0.17%) film taken at a roughness resolution ($4 \times 4\ \mu M^2$). For further details see text.

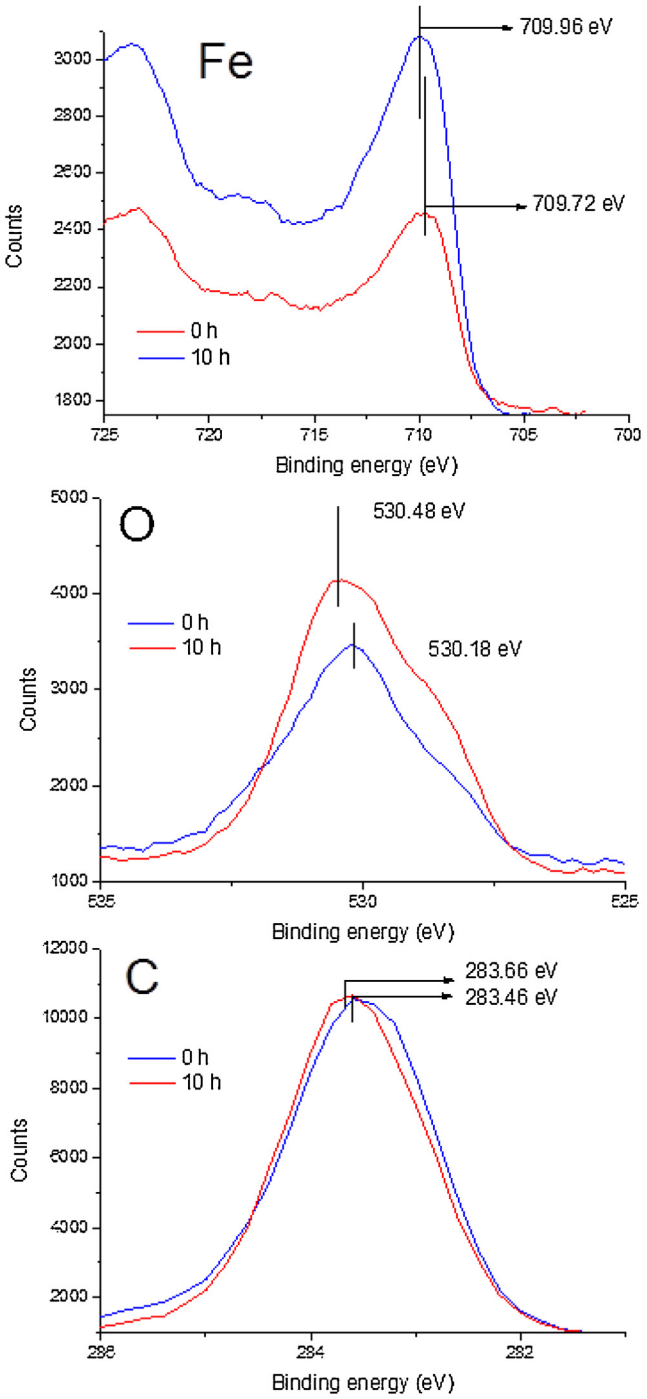

Fig. 9. XPS signals of Fe, O and C at time zero and after discoloration of a MB 4×10^{-5} (mol L^{-1} solution), under Suntest irradiation 50 mW/cm^{-2} on PE-FeOx films (0.30 Fe wt%).

Table 3
Surface percentage atomic concentration of PE-FeOx during MB discoloration determined by XPS. The PE-FeOx samples used were put in contact with MB for a short period in the dark (3s).

Reaction time (h)	C	N	O	S	Fe
PE	93.13		4.66		
0	82.03	2.33	13.02	1.03	1.17
2	74.43	3.20	18.91	1.37	1.52
10	76.81	0.20	18.12	0.36	2.28

FeOx does not accumulate intermediate residual species hindering the repetitive catalyst use. This observation is consistent with the XPS data described in the preceding paragraph suggesting that the catalytic destruction of the intermediates during MB-degradation is a fast process.

4. Conclusions

This study presents the first report on MB-degradation by an innovative PE-FeOx film inducing heterogeneous-homogeneous photo-Fenton reactions under low intensity sunlight/visible irradiation. The MB-degradation kinetics follows the kinetics typical of mass transfer controlled reactions on the PE-FeOx film. Evidence is presented for the specific nature of the oxidative radical intermediates intervening in the MB- degradation. The absence of vb hole (h^+) effects and the quasi-absence of light intensity effects suggest that the FeOx intervening as a semiconductor does not play an important role during MB-degradation. A mechanism leading to MB-degradation is suggested based on the experimental work carried out during this study. The PE-FeOx mediated Fenton catalysis leading to MB-degradation by a progressive co-participation of heterogeneous and homogeneous catalysis in solution. The PE-FeOx film surface microstructure was characterized by several overlapping surface techniques.

Acknowledgments

We thank the EPFL and the EC7th Limpid FP project (Grant No 3101177) for financial support and the COST Action MP1106 for interactive discussions during the course of this work. We thank S. Rtimi (EPFL) for the help with the experimental work during this study.

Appendix A. Supplementary data

Supplementary data associated with this article can be found, in the online version, at http://dx.doi.org/10.1016/j.apcata.2016.03.029.

References

[1] D. Dionysiou, A. Fujishima, X. Zhang, D. Tryk, Surf. Sci. Rep. 63 (2008) 515–582.
[2] M. Pelaez, N. Nolan, S. Pillai, M. Seery, P. Falaras, A.G. Kontos, Patrick S.M. Dunlop, J. Hamilton, J.-A. Byrne, K. O'Shea, M.H. Entezari, D.D. Dionysiou, Appl. Catal. B 125 (2012) 331–345.
[3] S. Banerjee, S.C. Pillai, P. Falaras, K. O'shea, J.-A. Byrne, D. Dionysiou, J. Phys. Chem. Lett. 5 (2014) 2543–2554.
[4] V. Etacheri, C. Di Valentin, J. Schneider, D. Bahnemann, S.J. Pillai, Photochem. Photobiol. C Revs. 25 (2015) 1–29.
[5] S. Banerjee, D. Dionysiou, S.C. Pillai, D.D. Dionysiou, Appl. Catal. B 176 (2015) 39.
[6] J. Schneider, M. Matsuoka, M. Takeuchi, J. Zhang, Y. Horiuchi, M. Anpo, D. Bahnemann, Chem. Rev. 118 (2014) 9919–9986.
[7] K. Hardee, A. Bard, J. Electrochem. Soc. 95 (1978) 215–224.
[8] S. Singh, H. Mahanlingam, P.K. Singh, Appl. Catal. A 462–463 (2013) 178–185.
[9] B. Ohtani, S. Adzuma, H. Miyadzu, S. Nishimoto, T. Kagiya, Polym. Degrad. Stab. 23 (1989) 271–278.
[10] L. Zhang, R. Dillert, D. Bahnemann, N. Vormoor, Energy Environ. 5 (2012) 7491–7507.
[11] A. Nozik, Ann. Rev. Phys. Chem. 29 (1978) 189–222.
[12] A. Mills, S. LeHunte, J. Photochem. Photobiol. A 108 (1997) 1–35.
[13] A. Mills, J. Wang, J. Photochem. Photobiol. A 127 (1999) 113–134.
[14] A. Houas, H. Lacheb, M. Kibsi, E. Elaloui, C. Guillard, J.-M. Herrmann, Appl. Catal. B 31 (2001) 145–157.
[15] J. Fernandez, J. Bandara, A. Lopez, Ph. Buffat, J. Kiwi, Langmuir 15 (1999) 185–192.
[16] M. Dhananjeyan, J. Kiwi, P. Albers, O. Enea, Helv. Chim. Acta 84 (2000) 3433–3445.
[17] J. Fernandez, M. Dhananjeyan, J. Kiwi, Y. Senuma, J. Hilborn, J. Phys. Chem. B 104 (2000) 5298–5301.
[18] S. Parra, I. Guasaquillo, O. Enea, J. Mielczarski, E. Mielczarski, L. Kiwi-Minsker, J. Kiwi, J. Phys. Chem. B. 107 (2003) 7026–7035.
[19] M. Dhananjeyan, J. Kiwi, R. Thampi, Chem. Comm (2000) 1443–1444.

[20] S. Rtimi, C. Pulgarin, R. Sanjines, J. Kiwi, RSC Adv. 5 (2015) 80203–80211.
[21] Handbook of X-ray Photoelectron Spectroscopy, in: C.D. Wagner, W.M. Riggs, L.E. Davis, G.E. Müllenberg (Eds.), Perkin-Elmer Corp, 1979, p. 19 (Phys. Electron Div.).
[22] J. Nogier, M. Delamar, P. Ruiz, M. Gratzel, R. Thampi, J. Kiwi, Catal. Today 20 (1994) 109–119.
[23] D.A. Shirley, Phys. Rev. B 5 (1972) 4709–4721.
[24] J.R. Bolton, C.E. Cotton, The UV-disinfection Handbook, Amer. Works Assoc., Denver, CO, 2008.
[25] G. Rupertvand, R. Bauer, J. Photochem. Photobiol. A 23 (1993) 75–78.
[26] A. Safarzadeh, J.R. Bolton, S.R. Carter, J. Adv. Oxid. Technol. 1 (1996) 18–21.
[27] P.V. Kamat, Chem. Rev. 93 (2011) 267–300.
[28] S. Rtimi, C. Pulgarin, R. Sanjines, J. Kiwi, Appl. Catal. B 162 (2015) 236–244.
[29] Y. Gak, V. Nadtochenko, J. Kiwi, J. Photochem. Photobiol A 116 (1998) 57–62.
[30] B. Kraeutler, C. Jaeger, A. Bard, J. Am. Chem. Soc. 100 (1978) 4903–4905.
[31] V. Nadtochenko, J. Kiwi, Inorg. Chem. 37 (1998) 5233–5238.
[32] W. Stumm, Aquatic Chemistry, John Wiley and Sons, New York, 1982.
[33] Aquatic and Surface Photochemistry, in: G.R. Helz, R. Zepp, D. Crosby (Eds.), CRC/Lewis Publishers, Boca Raton, FL, 1994, 552 p.